Femtoschool lectures

Marija Čuić

September 2024

1 Introduction

These lectures were devised for the first International School of Hadron Femtography, to be held at JLab between September 16th and September 25th, 2024, and are mostly based on the thesis [1]. The goal of these lectures is to offer an insight into how one would go from an observable related to an exclusive process to quantities related to the structure of the nucleon. I will give a brief introduction into exclusive processes and give an example of expanding GPDs in terms of conformal moments.

2 Exclusive processes

2.1 Deeply virtual Compton scattering

Deeply virtual Compton scattering (DVCS) is a hard *exclusive* process, symbolically written as

$$\ell(k_1) + N(P_1) \to \ell(k_2) + N(P_2) + \gamma(q_2). \tag{1}$$

Hard means that there is a large momentum carried by the virtual photon from the lepton to the nucleon, and exclusive means that we detect all of the products in the final state. After deep inelastic scattering (DIS), this process represents the next step in the pursuit of uncovering the structure of the proton. In this process, the incoming lepton emits a virtual photon, which then interacts with the constituents of the nucleon. In the final state we detect a lepton, a nucleon, and a real photon, which was emitted from the nucleon. The initial and final nucleons do not have the same momenta, but the nucleon remains intact, which together with the fact that the photon is emitted directly from the nucleon, allows for access of the three-dimensional structure of the nucleon. Because of the difference in the momenta of the initial and final nucleon, we refer to this process as being off-forward. When the process is forward, meaning that the momenta are thr same, we recover DIS.

Since the detectors only measure the products of the scattering, which are the lepton, nucleon and real photon in this case, DVCS interferes with another process with the same initial and final state, called the Bethe-Heitler process. In the Bethe-Heitler process, the final state photon is emitted from either the initial or the final lepton through Bremsstrahlung, and the interaction between the virtual photon and the nucleon is described by the electromagnetic form factors $F_{1,2}(Q^2)$. Both of these processes are depicted in figure 1 below.

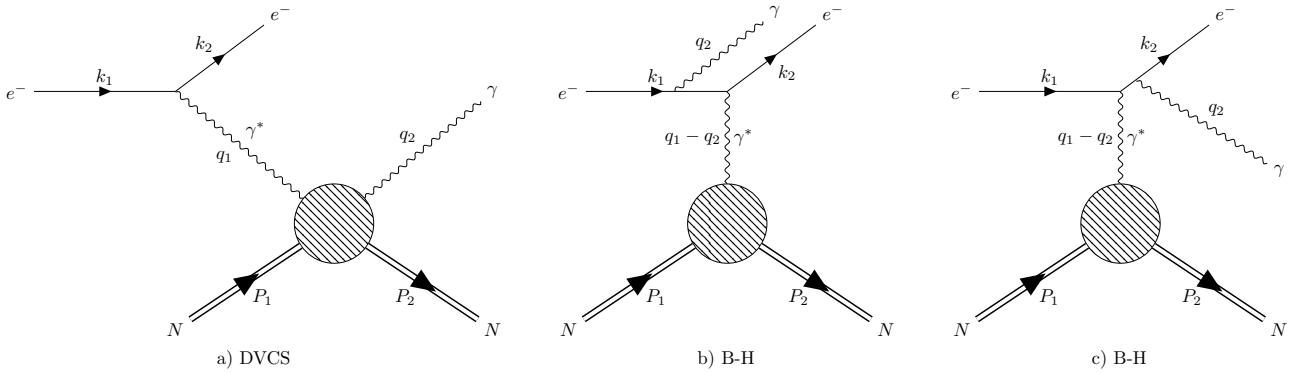

Figure 1: Deeply virtual Compton scattering and Bethe-Heitler process.

The amplitude for the process $\ell N \to \ell N \gamma$ is the sum of the amplitudes for DVCS and the Bethe-Heitler process, which means that the differential cross section is written as

$$\frac{\mathrm{d}\sigma}{\mathrm{d}x_{\mathrm{B}}\mathrm{d}y\mathrm{d}\left|\Delta^2\right|\mathrm{d}\phi\mathrm{d}\varphi} = \frac{\alpha^3 x_{\mathrm{B}} y}{16\pi^2 Q^2\sqrt{1+\epsilon^2}}\left|\frac{\mathcal{T}}{e^3}\right|^2, \tag{2}$$

where the amplitude is

$$|\mathcal{T}|^2 = |\mathcal{T}_{\rm DVCS}|^2 + |\mathcal{T}_{\rm BH}|^2 + \mathcal{I}, \tag{3}$$

and the interference term is given as

$$\mathcal{I} = \mathcal{T}^*_{\rm DVCS}\mathcal{T}_{\rm BH} + \mathcal{T}_{\rm DVCS}\mathcal{T}^*_{\rm BH}. \tag{4}$$

The cross section depends on 5 variables, because there are three particles in the final state which have 5 degrees of freedom. Some of these variables were introduced before, namely the opposite of the square four-momentum of the virtual photon $Q^2 = -q_1^2$, which now does not correspond to the momentum transfer to the hadron, and the Bjorken x defined as

$$x_{\rm B} = \frac{Q^2}{2P_1 \cdot q_1}. \tag{5}$$

The square of the four-momentum transfer to the hadron is given as

$$t = \Delta^2 = (P_2 - P_1)^2. \tag{6}$$

We also introduce the symmetric combinations of momenta

$$q = \frac{1}{2}(q_1 + q_2), \quad P = P_1 + P_2. \tag{7}$$

In order to describe the photon-proton scattering, we need three independent variables. We can choose from the following Lorentz scalars

$$\mathcal{Q}^2 = -q^2, \quad \xi_{\rm B} = \frac{\mathcal{Q}^2}{P \cdot q}, \quad \xi = -\frac{\Delta \cdot q}{P \cdot q}. \tag{8}$$

Note the different font between Q^2 and $\mathcal{Q}^2$. $\xi_{\rm B}$ is called the generalized Bjorken variable, and ξ is called the skewness. Skewness tells us how much the process is off-forward, meaning how much the struck parton momentum changes in the scattering. If the skewness is zero, we retrieve the forward Compton amplitude, and $\xi_{\rm B}$ coincides with $x_{\rm B}$. If additionally $\Delta = 0$, we recover deep inelastic scattering. We can also use the variables defined in DIS like $x_{\rm B}$ and

$$W^2 = (P_1 + q_1)^2. \tag{9}$$

In order to perturbatively approach this process, we employ the generalized Bjorken limit, which is given as

$$s = (P_1 + q_1)^2 \sim q_1^2 \to \infty, \quad -\Delta^2 \ll s, \quad x_{\rm B} = \text{fixed}, \tag{10}$$

and for DVCS (and DVMP, which we will define later) $\xi_{\rm B} \simeq \xi$. In this limit we have

$$Q^2 \simeq 2\mathcal{Q}^2, \quad \xi \simeq \frac{x_{\rm B}}{2 - x_{\rm B}}, \quad s \simeq 2P \cdot q. \tag{11}$$

We also introduce the notation for the average fraction of the longitudinal momentum of the proton carried by the struck parton x, which will be more precisely defined in the next chapter.

The limits on the momentum transfer are given by

$$\Delta^2_{\rm min,max} = -\frac{Q^2}{4x_{\rm B}\,(1 - x_{\rm B}) + \epsilon^2}\left[2\,(1 - x_{\rm B}) + \epsilon^2 \mp 2(1 - xB)\sqrt{1 + \epsilon^2}\right], \quad \varepsilon = 2x_{\rm B}\frac{M}{Q^2}. \tag{12}$$

The remaining two variables are the two angles ϕ and φ. In order to define them, we define the leptonic plane, which is subtended by the initial and final lepton 3-momenta, and the hadronic plane, which is subtended by the 3-momenta of the scattered nucleon and real photon. The angle ϕ is the angle between the leptonic plane and the recoiled nucleon 3-momentum, and φ is the angle between the scattered nucleon 3-momentum and its transverse polarization in the case of a polarized target. This frame is called the BKM frame [2] and is depicted in Figure 2 below.

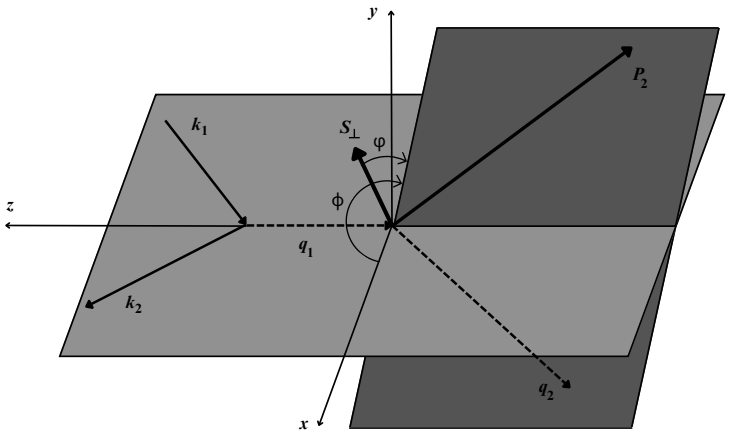

Figure 2: BKM reference frame. Adapted from [2].

In Figure 3 below we compare the squared amplitudes for DVCS and Bethe-Heitler, and their interference term. We can see that the Bethe-Heitler term dominates, that the cross section is symmetric with respect to the angle ϕ, and that the pure DVCS term does not depend on the angle.

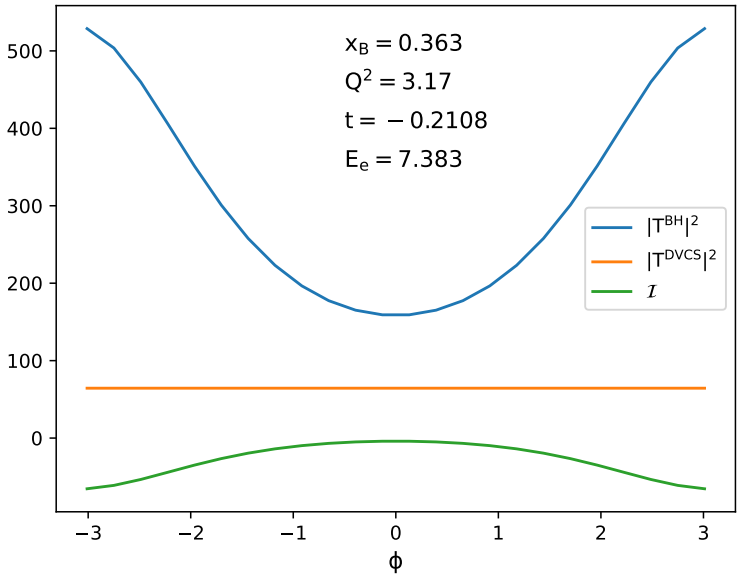

Figure 3: Comparison of $|\mathcal{T}_{\mathrm{BH}}|^2$, $|\mathcal{T}_{\mathrm{DVCS}}|^2$ and $\mathcal{I}$.

The DVCS cross section is parametrized in terms of complex functions called *Compton form factors* (CFFs), which are calculated as a convolution of the hard, perturbative part of the process, and the soft, non-perturbative part which gives access to the structure of the nucleon. This is not dissimilar to the extraction of PDFs in DIS, where experiments probe structure functions, which are convolutions of PDFs and the hard-scattering part. This phenomenon is called factorization, where the amplitude separates into the hard and soft part, which allows for the extraction of functions that describe the structure of the proton. In this instance, the soft functions are called *generalized parton distributions* (GPDs), which describe the transition from the initial nucleon to the final nucleon state. Factorization was proven in [3] for transversally polarized virtual photons.

The fact that the Bethe-Heitler process, which we can describe sufficiently well at the level of precision we have for DVCS, comes into the full $\ell N \to \ell N \gamma$ cross section provides a unique opportunity to access CFFs linearly and quadratically.

At leading order DVCS is described through the so-called hand-bag diagrams, which are depicted in Figure 4 below. In this part we observe only the hadronic part of the process, where at leading order we have the scattering of a virtual photon off a quark (or equivalently antiquark), which then emits a real photon and is absorbed back into the nucleon. Therefore, the initial and final nucleon have to be the same. Alternatively, this process could also be

thought of as an emission of a quark-antiquark pair from the nucleon, which absorbs the virtual photon and then annihilates into the final photon. If we accept the former interpretation, then we draw the s- and u-channels, where the fermion propagator in the hard subprocess carries the s and u four-momentum squared, respectively.

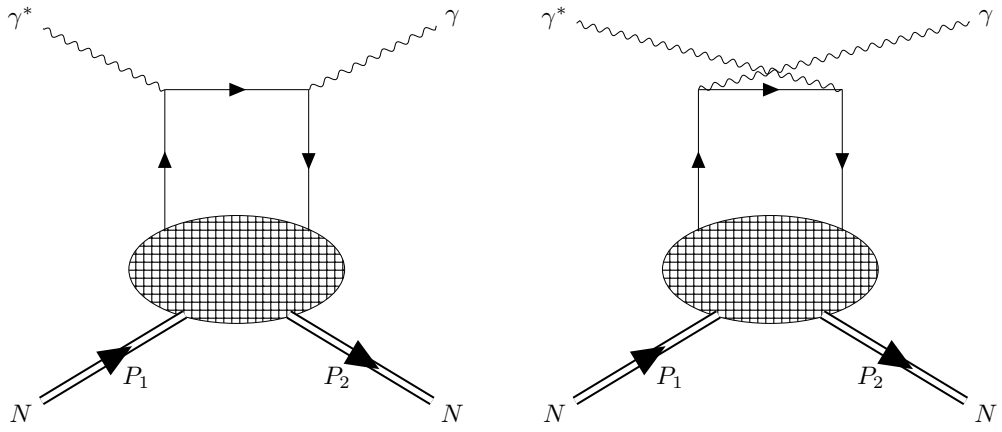

a) s-channel b) u-channel

Figure 4: Deeply virtual Compton scattering at leading order of perturbation theory.

Symbolically, we can write CFFs as

$$\mathcal{F}^A\left(\xi,\Delta^2,Q^2\right)=\int_{-1}^{1}\frac{\mathrm{d}x}{2\xi}{}^AT\left(x,\xi\middle|\alpha_{\mathrm{s}}\left(\mu_{\mathrm{R}}\right),\frac{Q^2}{\mu_{\mathrm{F}}^2}\right)F^A\left(x,\xi,\Delta^2,\mu_{\mathrm{F}}^2\right), \tag{13}$$

where the index A denotes all parton contributions, so $A\in\{u,d,s,\dots\mathrm{G}\}$. We have four types of CFFs, corresponding to the four GPDs that enter the amplitude at LO, which are $F\in\{H,E,\widetilde{H},\widetilde{E}\}$. The CFFs in the cross section are summed over all partons,

$$\mathcal{F}=\sum_A Q_A^2\mathcal{F}^A,\quad Q_{\mathrm{G}}^2=\frac{1}{N_f}\sum_q Q_q^2. \tag{14}$$

At leading order in α_S the CFFs take on the form

$$\begin{aligned}\mathcal{F}^A&=\int_{-1}^{+1}dx\left(\frac{1}{x-\xi-i\epsilon}-\frac{1}{x+\xi-i\epsilon}\right)F^A(x,\xi,t)\\&=\mathcal{P}\int_{-1}^{+1}dx\left(\frac{1}{x-\xi}-\frac{1}{x+\xi}\right)F^A(x,\xi,t)-i\pi(F^A(\xi,\xi,t)-F^A(-\xi,\xi,t))\end{aligned} \tag{15}$$

where the first term, the principle value of the integral, is the real part of the CFF, and the second part is the imaginary part (note that GPDs are real functions). We can see that the imaginary part is probed only on the so-called crossover line, where $x=\pm\xi$, and that it is proportional to the corresponding GPD.

The cross section can be calculated in several ways. In the approach of [2] the terms in the cross section (2) can be written as a decomposition into Fourier harmonics

$$\left|\mathcal{T}_{\mathrm{BH}}\right|^2=\frac{e^6}{x_{\mathrm{B}}^2y^2\left(1+\epsilon^2\right)^2\Delta^2\mathcal{P}_1(\phi)\mathcal{P}_2(\phi)}\left\{c_0^{\mathrm{BH}}+\sum_{n=1}^{2}c_n^{\mathrm{BH}}\cos(n\phi)+s_1^{\mathrm{BH}}\sin(\phi)\right\}, \tag{16}$$

$$\left|\mathcal{T}_{\mathrm{DVCS}}\right|^2=\frac{e^6}{y^2Q^2}\left\{c_0^{\mathrm{DVCS}}+\sum_{n=1}^{2}\left[c_n^{\mathrm{DVCS}}\cos(n\phi)+s_n^{\mathrm{DVCS}}\sin(n\phi)\right]\right\}, \tag{17}$$

$$\mathcal{I}=\frac{\pm e^6}{x_{\mathrm{B}}y^3\Delta^2\mathcal{P}_1(\phi)\mathcal{P}_2(\phi)}\left\{c_0^{I}+\sum_{n=1}^{3}\left[c_n^{I}\cos(n\phi)+s_n^{I}\sin(n\phi)\right]\right\}, \tag{18}$$

where we only keep the first few harmonics. Higher harmonics are suppressed by factors of $1/Q$, and correspond to contributions from higher twist. The sign ambiguity in the interference term comes from the charge sign of the lepton beam, + being for a negatively charged beam. The term $1/\mathcal{P}_1(\phi)\mathcal{P}_2(\phi)$ also has a ϕ dependence coming from the lepton propagators, which makes the Fourier analysis of experimental data more complicated.

Alternatively to this approach, we can calculate the cross section in terms of the helicity amplitudes, as outlined in [4]. We write the total cross section as

$$\sigma_{h\Lambda} = \Gamma \sum_{\Lambda'_\gamma, \Lambda'} \left(T^{h\Lambda'_\gamma}_{DVCS,\Lambda\Lambda'} \right)^* T^{h\Lambda'_\gamma}_{DVCS,\Lambda\Lambda'} = \Gamma \sum_{\Lambda^{(1)}_{\gamma^*}, \Lambda^{(2)}_{\gamma^*}} \mathcal{L}_h^{\Lambda^{(1)}_{\gamma^*}, \Lambda^{(2)}_{\gamma^*}} H_\Lambda^{\Lambda^{(1)}_{\gamma^*}, \Lambda^{(2)}_{\gamma^*}}, \tag{19}$$

where h and Λ are the helicities of the incoming lepton and proton, respectively, $\mathcal{L}$ is the lepton tensor, and H is the hadron tensor. The lepton tensor is written as

$$\mathcal{L}_h^{\Lambda^{(1)}_{\gamma^*}\Lambda^{(2)}_{\gamma^*}} = \sum_{\Lambda^{(1)}_{\gamma^*}, \Lambda^{(2)}_{\gamma^*}} A_h^{\Lambda^{(1)}_{\gamma^*}} A_h^{\Lambda^{(2)}_{\gamma^*}}, \tag{20}$$

where the lepton helicity amplitude is

$$A_h^{\Lambda_{\gamma^*}} = \frac{1}{Q^2} \overline{u}(k', h) \gamma^\mu u(k, h) \left(\varepsilon_\mu^{\Lambda_{\gamma^*}}(q) \right)^*. \tag{21}$$

The hadron tensor is calculated as

$$H_\Lambda^{\Lambda^{(1)}_{\gamma^*}\Lambda^{(2)}_{\gamma^*}} = \sum_{\Lambda'} F_{\Lambda\Lambda'}^{\Lambda^{(1)}_{\gamma^*}\Lambda^{(2)}_{\gamma^*}}, \tag{22}$$

where the hadron helicity amplitudes are defined as

$$F_{\Lambda\Lambda'}^{\Lambda^{(1)}_{\gamma^*}\Lambda^{(2)}_{\gamma^*}} = \sum_{\Lambda'_\gamma} \left[f_{\Lambda,\Lambda'}^{\Lambda^{(1)}_{\gamma^*}, \Lambda'_\gamma} \right]^* f_{\Lambda,\Lambda'}^{\Lambda^{(2)}_{\gamma^*}, \Lambda'_\gamma}. \tag{23}$$

The total cross section is then

$$\begin{aligned}
\frac{d^5\sigma_{DVCS}}{dx_{Bj} dQ^2 d|t| d\phi d\phi_S} &= \Gamma \left| T_{DVCS} \right|^2 \\
&= \frac{\Gamma}{Q^2(1-\epsilon)} \Big\{ F_{UU,T} + \epsilon F_{UU,L} + \epsilon \cos 2\phi F_{UU}^{\cos 2\phi} \\
&+ \sqrt{\epsilon(\epsilon+1)} \cos\phi F_{UU}^{\cos\phi} + (2h)\sqrt{2\epsilon(1-\epsilon)} \sin\phi F_{LU}^{\sin\phi} \\
&+ (2\Lambda) \left[\sqrt{\epsilon(\epsilon+1)} \sin\phi F_{UL}^{\sin\phi} + \epsilon \sin 2\phi F_{UL}^{\sin 2\phi} \right. \\
&\left. + (2h) \left(\sqrt{1-\epsilon^2} F_{LL} + 2\sqrt{\epsilon(1-\epsilon)} \cos\phi F_{LL}^{\cos\phi} \right) \right] \\
&+ (2\Lambda_T) \left[\sin(\phi - \phi_S) \left(F_{UT,T}^{\sin(\phi-\phi_S)} + \epsilon F_{UT,L}^{\sin(\phi-\phi_S)} \right) \right. \\
&+ \epsilon \sin(\phi + \phi_S) F_{UT}^{\sin(\phi+\phi_S)} + \epsilon \sin(3\phi - \phi_S) F_{UT}^{\sin(3\phi-\phi_S)} \\
&\left. + \sqrt{2\epsilon(1+\epsilon)} \left(\sin\phi_S F_{UT}^{\sin\phi_S} + \sin(2\phi - \phi_S) F_{UT}^{\sin(2\phi-\phi_S)} \right) \right] \\
&+ (2h)(2\Lambda_T) \left[\sqrt{1-\epsilon^2} \cos(\phi - \phi_S) F_{LT}^{\cos(\phi-\phi_S)} \right. \\
&+ \sqrt{2\epsilon(1-\epsilon)} \cos\phi_S F_{LT}^{\cos\phi_S} \\
&\left. + \sqrt{2\epsilon(1-\epsilon)} \cos(2\phi - \phi_S) F_{LT}^{\cos(2\phi-\phi_S)} \right] \Big\}.
\end{aligned} \tag{24}$$

The unpolarized DVCS amplitude can be written as

$$\begin{aligned}
|\mathcal{T}_{\rm DVCS}|^2 = \frac{2\left(2 - 2y + y^2\right)}{y^2 Q^2 \left(2 - x_{\rm B}\right)^2} \Big[& 4\left(1 - x_{\rm B}\right) \left(|\mathcal{H}|^2 + |\widetilde{\mathcal{H}}|^2 \right) - \left(x_{\rm B}^2 + \left(2 - x_{\rm B}\right)^2 \frac{\Delta^2}{4M^2} \right) |\mathcal{E}|^2 \\
& - x_{\rm B}^2 \left(\mathcal{H}\mathcal{E}^* + \mathcal{E}\mathcal{H}^* + \widetilde{\mathcal{H}}\widetilde{\mathcal{E}}^* + \widetilde{\mathcal{E}}\widetilde{\mathcal{H}}^* \right) - x_{\rm B}^2 \frac{\Delta^2}{4M^2} |\widetilde{\mathcal{E}}|^2 \Big], \quad y = \frac{Q^2}{xs}.
\end{aligned} \tag{25}$$

Let us illustrate how the LO hard coefficient arises, and what role the angle ϕ plays in the form of the cross section. If we take a look at the hadronic part of the handbag diagram from Figure 4, specifically the s-channel on the left, we can see that the amplitude will contain the structure

$$\varepsilon_\mu^{\Lambda_{\gamma^*}}(q_1) \gamma^\mu \frac{1}{\not{k}_1 + \not{q}_1} \gamma^\nu \left(\varepsilon_\nu^{\Lambda_{\gamma'}}(q_2) \right)^* = \gamma^\mu \frac{\not{k}_1 + \not{q}_1}{(k_1 + q_1)^2} \gamma^\nu \varepsilon_\mu^{\Lambda_{\gamma^*}}(q_1) \left(\varepsilon_\nu^{\Lambda_{\gamma'}}(q_2) \right)^*. \tag{26}$$

We have ignored the mass of the quark in the denominator. If we take a look at the denominator, we find

$$(k_1+q_1)^2 = k_1^2 + 2k_1\cdot q_1 + q_1^2 \approx 2k_1\cdot q_1 - Q^2 = Q^2\left(-1+\frac{2k_1\cdot q_1}{Q^2}\right). \tag{27}$$

We have again ignored the mass of the quark by setting $k^2=0$. By definition, the momentum of the struck parton can be written as $(x+\xi)P/2$, where P is the total nucleon momentum, as defined previously. If we write

$$q_1 = q + \frac{\Delta}{2}, \tag{28}$$

use the first relation in (11) and the fact that $P\cdot\Delta = 0$, we have

$$Q^2\left(-1+\frac{2k_1\cdot q_1}{Q^2}\right) = Q^2\left(-1+(x+\xi)\frac{P\cdot q}{2\mathcal{Q}^2}\right) = Q^2\left(-1+(x+\xi)\frac{1}{2\xi_{\mathrm{B}}}\right) \approx \frac{Q^2}{2\xi}(x-\xi). \tag{29}$$

In the numerator, we will disregard the contribution from $\not{k}$ since it is much smaller than q. If we look at the coordinate frame from 2, we can see that the virtual photon is moving in the direction $-\hat{z}$. In terms of light-cone coordinates, the momentum of the virtual photon is given as

$$q^\mu = (q^+, q^-, \boldsymbol{q}_\perp), \quad q^\pm = \frac{q^0 \pm q^3}{\sqrt{2}}, \quad \boldsymbol{q}_\perp = 0. \tag{30}$$

Since the photon has large virtuality, we can assume $q^0 \approx -q^3$. This means that $q^+ \approx 0$. Therefore, the Dirac structure in the numerator becomes

$$\gamma^\mu\gamma^+\gamma^\nu = g^{\mu+}\gamma^\nu - g^{\mu\nu}\gamma^+ + g^{\nu+}\gamma^\mu + \mathrm{i}\epsilon^{\sigma\mu+\nu}\gamma_5\gamma_\sigma. \tag{31}$$

Given that the outgoing photon is real, its polarization can only be transverse, so the index ν can only take on the values 1 and 2, which we will write as i. In terms of the light-cone coordinates, this index lives in the transverse space, so it is orthogonal to the indices $\pm$. We therefore have

$$\gamma^\mu\gamma^+\gamma^i = g^{\mu+}\gamma^i - g^{\mu i}\gamma^+ + g^{i+}\gamma^\mu + \mathrm{i}\epsilon^{\sigma\mu+i}\gamma_5\gamma_\sigma = g^{\mu+}\gamma^i - g^{\mu i}\gamma^+ + \mathrm{i}\epsilon^{\sigma\mu+i}\gamma_5\gamma_\sigma. \tag{32}$$

It can be shown that the last term will correspond to axial GPDs, both at the twist-2 and twist-3 level, the first term to twist-3 contributions, and the second term to twist-2. Due to the term $g^{\mu i}$, at the twist-2 level the polarization of the virtual photon has to be transverse, whereas twist-3 will involve a longitudinally polarized virtual photon.

Since we are looking at the hadronic part of the process, which happens in the so-called hadronic plane, we will write the polarization of the virtual photon as

$$\varepsilon^{\pm1}(q)_\mu = \frac{e^{\pm i\phi}}{\sqrt{2}}(0,\mp1,i,0), \quad \varepsilon^0(q)_\mu = \frac{1}{Q}(q^0,0,0,|\boldsymbol{q}|). \tag{33}$$

The hadronic part of the cross section is calculated as

$$\sum_{\Lambda^{(1)}_{\gamma^*}\Lambda^{(2)}_{\gamma^*}\Lambda'_\gamma\Lambda'} \left[f^{\Lambda^{(1)}_{\gamma^*},\Lambda'_\gamma}_{\Lambda,\Lambda'}\right]^* f^{\Lambda^{(2)}_{\gamma^*},\Lambda'_\gamma}_{\Lambda,\Lambda'}, \tag{34}$$

where we sum over the polarizations of the outgoing photon and nucleon, since this is how most observables for DVCS are measured. Since the polarization of the virtual photon is not measured, it can in principle differ between the amplitude and its conjugate. We can therefore have combinations where $\Lambda^{(1)}_{\gamma^*} = \Lambda^{(2)}_{\gamma^*} = i$, which will not incur a phase dependence, since we will have $\varepsilon^a(\varepsilon^a)^*$. If we have $\Lambda^{(1)}_{\gamma^*} = 0$ and $\Lambda^{(2)}_{\gamma^*} = i$, we will have a factor of $e^{\pm i\phi}$. We know that a longitudinal virtual photon corresponds to twist-3. If we have $\Lambda^{(1)}_{\gamma^*} = \pm1$ and $\Lambda^{(2)}_{\gamma^*} = \mp1$, then we have a factor $e^{\pm i2\phi}$. This case corresponds to the gluon transversity GPDs, which describe a helicity flip by two units. They are techically twist-2, but are suppressed by α_S since they involve gluons. The case $\Lambda^{(1)}_{\gamma^*} = \Lambda^{(2)}_{\gamma^*} = 0$ corresponds to twist 4. This is a quick and dirty way to illustrate how twist expansion corresponds to expansion in terms of $\sin(n\phi)$ and $\cos(n\phi)$ functions.

2.2 Deeply virtual meson production

Deeply virtual meson production (DVMP) is another hard exclusive process that gives access to GPDs, and it is symbolically written as

$$\ell(k_1) + N(P_1) \to \ell(k_2) + N'(P_2) + M(q_2). \tag{35}$$

In the final state we now have a meson instead of a photon like in DVCS, and depending on the meson, the final state hadron does not have to be the same as the initial hadron. The process is depicted in Figure 5 below.

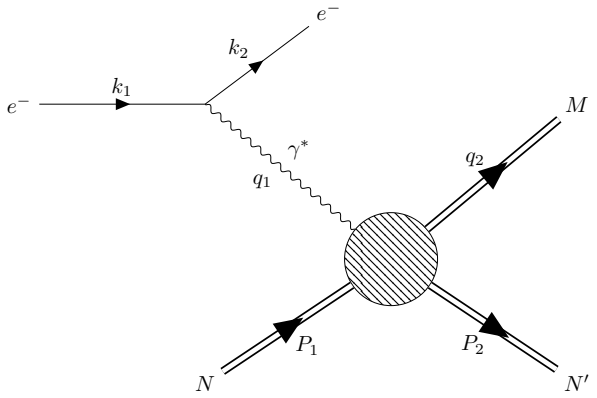

Figure 5: Deeply virtual meson production.

We again rely on factorization, which was proven for light pseudoscalar mesons and longitudinally polarized vector mesons in [5]. At LO, many channels have been studied [6, 7, 8, 9, 10, 11, 12, 13]. Some of these studies have been extended to NLO accuracy [14, 15, 16, 17, 18].

At leading order, we observe two types of diagrams, depicted in Figure 6 below.

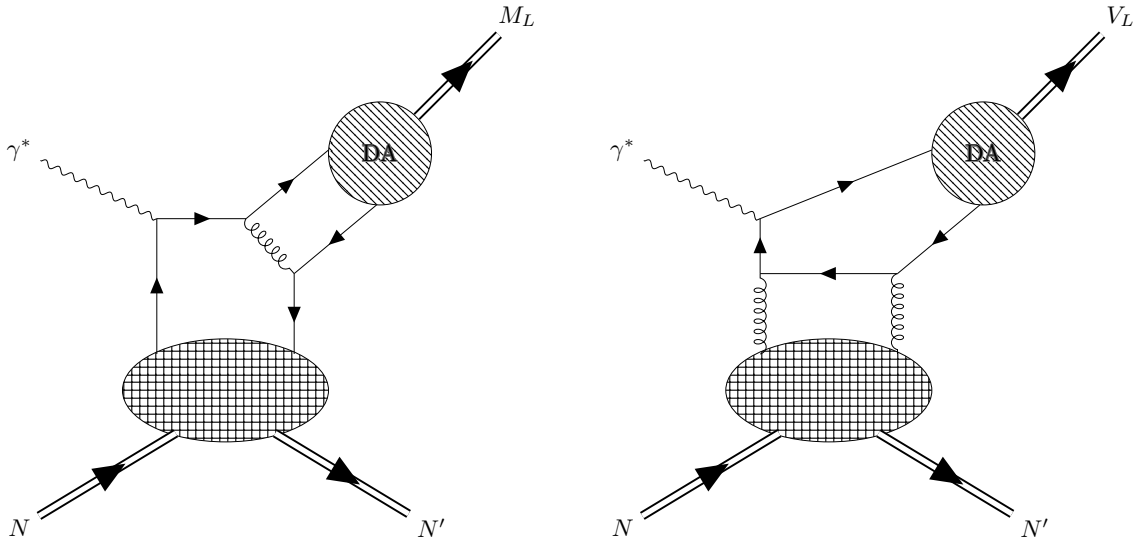

a) quark subprocess b) gluon subprocess

Figure 6: Deeply virtual meson production at leading order of perturbation theory.

Note that at LO DVMP has one less QED vertex in comparison to DVCS, because there is no final-state photon. The DVMP cross section is therefore larger than the DVCS cross section. Also, gluons enter DVMP at leading order, but for DVCS they appear in next-to-leading order corrections. In the case of the quark subprocess, we need a gluon in order to bind a quark and antiquark into the final meson state. This diagram can be observed in two ways. We can look at it as a quark emitted from the nucleon, which absorbs the virtual photon and emits a gluon, which then breaks up into a quark and antiquark. This quark is absorbed into the nucleon, and the original quark binds to the antiquark emitted from the gluon into the final-state meson. Alternatively, a quark-antiquark pair are emitted from the nucleon, they absorb the virtual photon and bind into the final-state meson by exchanging a gluon. Both of these processes can also be produced in the u-channel.

Since we only have one QED vertex, the amplitude is described by the transition amplitude

$$A_\mu = \int \mathrm{d}^4 z e^{-iq_1 z} \left\langle q_2 \mathrm{P}_2 \left| j_\mu(z) \right| \mathrm{P}_1 \right\rangle , \tag{36}$$

which we use to calculate the cross section. This time the cross section, which is

$$\frac{\mathrm{d}^2\sigma^{\gamma_{\mathrm{L}}^*\longmapsto MN'}}{\mathrm{d}\Delta^2\ \mathrm{d}\phi} = \frac{\alpha_{\mathrm{em}}x_{\mathrm{B}}^2y^2}{32\pi Q^2\sqrt{1+\epsilon^2}}\frac{1}{1-y}\left|\mathcal{T}^{\mathrm{DVMP}}\right|^2, \tag{37}$$

with

$$\left|\mathcal{T}^{\mathrm{V_L}}\right|^2 = 16\frac{1-y}{y^2\left(2-x_{\mathrm{B}}\right)^2}\left[4\left(1-x_{\mathrm{B}}\right)|\mathcal{H}|^2 - x_{\mathrm{B}}^2\left(\mathcal{H}\mathcal{E}^* + \mathcal{E}\mathcal{H}^*\right) - \left(x_{\mathrm{B}}^2 + \left(2-x_{\mathrm{B}}\right)^2\frac{\Delta^2}{4M^2}\right)|\mathcal{E}|^2\right], \tag{38}$$

$$\left|\mathcal{T}^{\mathrm{PS}}\right|^2 = 16\frac{1-y}{y^2\left(2-x_{\mathrm{B}}\right)^2}\left[4\left(1-x_{\mathrm{B}}\right)|\widetilde{\mathcal{H}}|^2 - x_{\mathrm{B}}^2\left(\widetilde{\mathcal{H}}\widetilde{\mathcal{E}}^* + \widetilde{\mathcal{E}}\widetilde{\mathcal{H}}^*\right) - x_{\mathrm{B}}^2\frac{\Delta^2}{4M^2}|\widetilde{\mathcal{E}}|^2\right] \tag{39}$$

is given in terms of *transition form factors* (TFFs). Symbolically, we can write them as

$$\mathcal{F}^A\left(\xi,\Delta^2,Q^2\right) = \frac{fC_{\mathrm{F}}}{QN_{\mathrm{c}}}\int_{-1}^{1}\frac{\mathrm{d}x}{2\xi}\int_0^1\ \mathrm{d}v\varphi(v)^{\mathrm{A}}T\left(x,v,\xi\middle|\alpha_{\mathrm{s}}\left(\mu_{\mathrm{R}}\right),\frac{Q^2}{\mu_{\mathrm{F}}^2},\frac{Q^2}{\mu_\varphi^2},\frac{Q^2}{\mu_{\mathrm{R}}^2}\right)F^A\left(x,\xi,\Delta^2,\mu_{\mathrm{F}}^2\right). \tag{40}$$

TFFs are factorized into three parts, one being the standard hard-scale amplitude T, another being the soft-scale GPDs F, and the last one being the soft-scale distribution amplitude (DA) $\phi(v)$. The distribution amplitude describes the transition from vacuum to the final-state meson. The variable v is now the fraction of the longitudinal momentum of the meson. The distribution amplitude represents another soft-scale component of the process which we cannot access from first principles.

Due to an intricate flavor structure of the final-state mesons, we can access several flavor combinations of GPDs through various DVMP measurements. We expect these GPDs to be universal for all DVCS and DVMP variations, as well as other processes that probe GPDs (or more precisely, their convolutions).

2.3 Other processes

Other exclusive processes that probe GPDs are for example time-like Compton scattering (TCS) [19], double DVCS (DDVCS) [20, 21, 22], and processes that have four or more particles in the final state, such as a photon and a meson, or two mesons alongside the nucleon and lepton. In TCS the incoming photon is real, and the outgoing photon is virtual. This process has a similar hard-scale amplitude as DVCS and its analysis could also offer a test for GPD universality. In DDVCS both the incoming and outgoing photons are virtual, so DVCS and TCS are limiting cases of this process. Aside from accessing different GPDs, these processes also offer access to different kinematic regions. Specifically, DDVCS offers access to GPDs outside the crossover line. These processes are depicted in Figure 7 below.

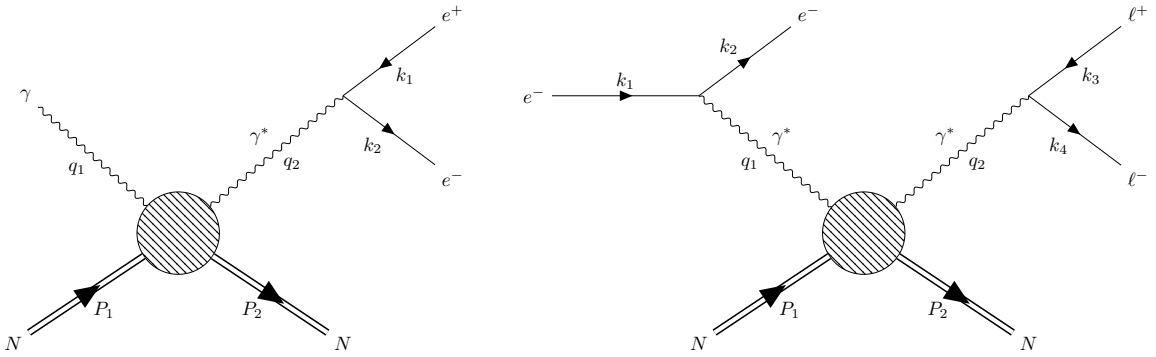

Figure 7: TCS and DDVCS.

3 Dispersion relations

Dispersion relations come from analyticity and causality considerations of Compton form factors and they relate their real and imaginary part [23, 24]. We give an example for the CFF $\mathcal{H}$

$$\mathfrak{Re}\mathcal{H}\left(\xi,t,Q^2\right) = \frac{1}{\pi}\ \mathrm{P.V.}\ \int_0^1\mathrm{d}\xi'\mathfrak{Im}\mathcal{H}\left(\xi',t,Q^2\right)\left(\frac{1}{\xi-\xi'}-\frac{1}{\xi+\xi'}\right)+\Delta_{\mathcal{H}}\left(t,Q^2\right), \tag{41}$$

where $\Delta_{\mathcal{H}}(t,Q^2)$ is a subtraction constant that does not depend on the skewness. Expression (41) is formally a dispersion relation with one subtraction, referring to the subtraction constant Δ, which does not depend on the

skewness. This subtraction constant is necessary to cancel out divergences at the point $\xi = 0$ and $x = 0$ that occur in CFFs. It is worth noting that the integral over ξ' goes from 0 to 1, but skewness is bounded by

$$|\xi| \leq \frac{\sqrt{-t}}{\sqrt{-t+4M^2}}, \tag{42}$$

and for most experimental setups this means that the integral (41) will go out of the physical domain where CFFs are defined. Therefore, analytic continuation is necessary in order to extract knowledge on the subtraction constant.

Dispersion relations belong in the same realm of scattering theory as Regge theory, where various analyticity and causality properties, asymptotic behavior, poles and cuts are used in order to study scattering amplitudes and draw conclusions on their functional form, without ever getting into the underlying non-perturbative functions. A lot of state-of-the-art analysis of CFFs is done using machine learning.

4 Observables

Using the experimental data for the differential cross section, total cross section and various asymmetries for proton and neutron DVCS, we access the twist-two Compton form factors, $\mathcal{H}$, $\mathcal{E}$, $\widetilde{\mathcal{H}}$, $\widetilde{\mathcal{E}}$. The asymmetries are generally denoted as A_{BC}, where the first letter denotes the polarization of the beam, and the second the polarization of the target, and they can have values U for unpolarized, L for longitudinally polarized and T for transversally polarized.

One of these observables is the beam spin asymmetry, denoted BSA or A_{LU}, where the beam is longitudinally polarized, and the target is unpolarized. It is defined as

$$\begin{aligned} A_{\mathrm{LU}}(\phi) &= \frac{\mathrm{d}\sigma^{\uparrow}(\phi) - \mathrm{d}\sigma^{\downarrow}(\phi)}{\mathrm{d}\sigma^{\uparrow}(\phi) + \mathrm{d}\sigma^{\downarrow}(\phi)} \\ &\propto \mathfrak{Im}\left\{ F_1\mathcal{H} + \xi\left(F_1+F_2\right)\widetilde{\mathcal{H}} - \frac{\Delta^2}{4M^2}F_2\mathcal{E} \right\}\sin(\phi). \end{aligned} \tag{43}$$

Here $\sigma^{\uparrow}$ denotes the cross section where the beam is polarized in the direction of the flow of leptons, and $\sigma^{\downarrow}$ denotes the cross section where the beam is polarized in the opposite direction to the flow of leptons. For typical kinematics the first sine harmonic is dominant, so we usually perform a Fourier transform and just observe the amplitude of the BSA. This quantity is particularly sensitive to the imaginary part of the CFF $\mathcal{H}$.

Another set of data that is used is for longitudinal target spin asymmetry, denoted as TSA or A_{UL}, which is given as

$$\begin{aligned} A_{\mathrm{UL}}(\phi) &= \frac{\mathrm{d}\sigma^{\Rightarrow}(\phi) - \mathrm{d}\sigma^{\Leftarrow}(\phi)}{\mathrm{d}\sigma^{\Rightarrow}(\phi) + \mathrm{d}\sigma^{\Leftarrow}(\phi)} \\ &\propto \mathfrak{Im}\left[F_1\widetilde{\mathcal{H}} + \xi\left(F_1+F_2\right)\left(\mathcal{H} + \frac{x_{\mathrm{B}}}{2}\mathcal{E}\right) - \xi\left(\frac{x_{\mathrm{B}}}{2}F_1 + \frac{t}{4M^2}F_2\right)\widetilde{\mathcal{E}} \right]\sin(\phi), \end{aligned} \tag{44}$$

where $\sigma^{\Rightarrow}$ denotes the cross section where the target is polarized in the direction of the flow of leptons, and $\sigma^{\Leftarrow}$ denotes the cross section where the target is polarized in the opposite direction to the flow of leptons. This quantity is sensitive to the imaginary parts of $\mathcal{H}$ and $\widetilde{\mathcal{H}}$.

The double spin asymmetry, denoted as BTSA or A_{LL}, which is given as

$$\begin{aligned} A_{\mathrm{LL}}(\phi) &= \frac{\mathrm{d}\sigma^{\uparrow\Uparrow}(\phi) - \mathrm{d}\sigma^{\downarrow\Uparrow}(\phi) - \mathrm{d}\sigma^{\uparrow\Downarrow}(\phi) + \mathrm{d}\sigma^{\downarrow\Downarrow}(\phi)}{\mathrm{d}\sigma^{\uparrow\Uparrow}(\phi) + \mathrm{d}\sigma^{\downarrow\Uparrow}(\phi) + \mathrm{d}\sigma^{\uparrow\Downarrow}(\phi) + \mathrm{d}\sigma^{\downarrow\Downarrow}(\phi)} \\ &\propto \mathfrak{Re}\left[F_1\widetilde{\mathcal{H}} + \xi\left(F_1+F_2\right)\left(\mathcal{H} + \frac{x_{\mathrm{B}}}{2}\mathcal{E}\right) - \xi\left(\frac{x_{\mathrm{B}}}{2}F_1 + \frac{t}{4M^2}F_2\right)\widetilde{\mathcal{E}} \right]\cos\phi + BH, \end{aligned} \tag{45}$$

is also used in the analysis. Here the arrow $\uparrow$ denotes that the spin of the leptons is polarized in the direction of the beam, and $\downarrow$ means that it is polarized in the opposite direction. The same is valid for the spin of the target, denoted with the double arrow. This quantity is sensitive to the Bethe-Heitler and interference contributions, but at certain kinematics it can be sensitive to real parts of $\mathcal{H}$ and $\widetilde{\mathcal{H}}$.

The unpolarized beam-charge asymmetry, or A_{C}, is given as

$$\begin{aligned} A_{\mathrm{C}} &= \frac{\sigma^{+}_{\mathrm{UU}} - \sigma^{-}_{\mathrm{UU}}}{\sigma^{+}_{\mathrm{UU}} + \sigma^{-}_{\mathrm{UU}}} \\ &\propto \mathfrak{Re}\left[F_1\mathcal{H} + \xi\left(F_1+F_2\right)\widetilde{\mathcal{H}} - \frac{\Delta^2}{4M^2}F_2\mathcal{E} \right]\cos(n\phi), \quad n \in \{0,1\}. \end{aligned} \tag{46}$$

Here σ^{+}_{UU} denotes the 4-fold unpolarized cross section with a positron beam, and σ^{+}_{UU} denotes the 4-fold unpolarized cross section with an electron beam. We can see that this asymmetry probes the same combination of CFFs as the beam-spin asymmetry, but in this instance it is the real component.

Other quantities that were used in our analysis are the beam spin sum BSS, which is unpolarized, and the beam spin difference BSD, which is helicity-dependent. They are given as

$$\mathrm{d}^4\sigma = \frac{1}{2}\left[\frac{\mathrm{d}^4\sigma(\lambda=+1)}{\mathrm{d}Q^2\mathrm{d}x_{\mathrm{B}}\mathrm{d}t\mathrm{d}\phi} + \frac{\mathrm{d}^4\sigma(\lambda=-1)}{\mathrm{d}Q^2\mathrm{d}x_{\mathrm{B}}\mathrm{d}t\mathrm{d}\phi}\right],$$
$$\Delta^4\sigma = \frac{1}{2}\left[\frac{\mathrm{d}^4\sigma(\lambda=+1)}{\mathrm{d}Q^2\mathrm{d}x_{\mathrm{B}}\mathrm{d}t\mathrm{d}\phi} - \frac{\mathrm{d}^4\sigma(\lambda=-1)}{\mathrm{d}Q^2\mathrm{d}x_{\mathrm{B}}\mathrm{d}t\mathrm{d}\phi}\right].$$

The helicity-independent cross section depends mostly on the real part of the same coefficient as the BSA, and the helicity-dependent cross section depends mostly on the imaginary part of that coefficient.

For a set of kinematic variables given in Table 1 below, we can obtain the contributions of CFFs to various observables, given in Table 2.

Experiment	Kinematics		
	x_{B}	$Q^2\,[\mathrm{GeV}^2]$	$t\,[\mathrm{GeV}^2]$
HERMES	0.09	2.50	-0.12
CLAS	0.19	1.25	-0.19
HALL A	0.36	2.30	-0.23
HERA	0.001	8.00	-0.30

Table 1: Typical kinematics used for experiments. Taken from [25].

Experiment	Observable	Normalized CFF dependence
HERMES	$A_{\mathrm{C}}^{\cos 0\phi}$	$\mathfrak{Re}\mathcal{H} + 0.06\mathfrak{Re}\mathcal{E} + 0.24\mathfrak{Re}\widetilde{\mathcal{H}}$
	$A_{\mathrm{C}}^{\cos\phi}$	$\mathfrak{Re}\mathcal{H} + 0.05\mathfrak{Re}\mathcal{E} + 0.15\mathfrak{Re}\widetilde{\mathcal{H}}$
	$A_{\mathrm{LU,I}}^{\sin\phi}$	$\mathfrak{Im}\mathcal{H} + 0.05\mathfrak{Im}\mathcal{E} + 0.12\mathfrak{Im}\widetilde{\mathcal{H}}$
	$A_{\mathrm{UL}}^{+,\sin\phi}$	$\mathfrak{Im}\widetilde{\mathcal{H}} + 0.10\mathfrak{Im}\mathcal{H} + 0.01\mathfrak{Im}\mathcal{E}$
	$A_{\mathrm{UL}}^{+,\sin 2\phi}$	$\mathfrak{Im}\widetilde{\mathcal{H}} - 0.97\mathfrak{Im}\mathcal{H} + 0.49\mathfrak{Im}\mathcal{E} - 0.03\mathfrak{Im}\widetilde{\mathcal{E}}$
	$A_{\mathrm{LL}}^{+,\cos 0\phi}$	$1 + 0.05\mathfrak{Re}\widetilde{\mathcal{H}} + 0.01\mathfrak{Re}\mathcal{H}$
	$A_{\mathrm{LL}}^{+,\cos\phi}$	$1 + 0.79\mathfrak{Re}\widetilde{\mathcal{H}} + 0.11\mathfrak{Im}\mathcal{H}$
	$A_{\mathrm{UT,DVCS}}^{\sin(\phi-\phi_S)}$	$\mathfrak{Im}\mathcal{H}\mathfrak{Re}\mathcal{E} - \mathfrak{Im}\mathcal{E}\mathfrak{Re}\mathcal{H}$
	$A_{\mathrm{UT,I}}^{\sin(\phi-\phi_S)\cos\phi}$	$\mathfrak{Im}\mathcal{H} - 0.56\mathfrak{Im}\mathcal{E} - 0.12\mathfrak{Im}\widetilde{\mathcal{H}}$
CLAS	$A_{\mathrm{LU}}^{-,\sin\phi}$	$\mathfrak{Im}\mathcal{H} + 0.06\mathfrak{Im}\mathcal{E} + 0.21\mathfrak{Im}\widetilde{\mathcal{H}}$
	$A_{\mathrm{UL}}^{-,\sin\phi}$	$\mathfrak{Im}\widetilde{\mathcal{H}} + 0.12\mathfrak{Im}\mathcal{H} + 0.04\mathfrak{Im}\mathcal{E}$
	$A_{\mathrm{UL}}^{-,\sin 2\phi}$	$\mathfrak{Im}\widetilde{\mathcal{H}} - 0.79\mathfrak{Im}\mathcal{H} + 0.30\mathfrak{Im}\mathcal{E} - 0.05\mathfrak{Im}\widetilde{\mathcal{E}}$
HALL A	$\Delta\sigma^{\sin\phi}$	$\mathfrak{Im}\mathcal{H} + 0.07\mathfrak{Im}\mathcal{E} + 0.47\mathfrak{Im}\widetilde{\mathcal{H}}$
	$\sigma^{\cos 0\phi}$	$1 + 0.05\mathfrak{Re}\mathcal{H} + 0.007\mathcal{H}\mathcal{H}^*$
	$\sigma^{\cos\phi}$	$1 + 0.12\mathfrak{Re}\mathcal{H} + 0.05\mathfrak{Re}\widetilde{\mathcal{H}}$
HERA	σ_{DVCS}	$\mathcal{H}\mathcal{H}^* + 0.09\mathcal{E}\mathcal{E}^* + \widetilde{\mathcal{H}}\widetilde{\mathcal{H}}^*$

Table 2: Dependence of observables on CFFs, normalized to the highest coefficient. The coefficients are evaluated at the kinematics from Table 1. Coefficients smaller than 1% are not kept, except for the Hall A cross section. Taken from [25].

5 Conformal partial wave expansion

In this work we approach GPD modeling in the space of conformal moments, and the goal of this section is to derive a representation of GPDs in the conformal space. Analogous steps were taken in modeling PDFs, where an expansion in terms of Mellin moments was used

$$f_j^q = \int_{-1}^{1} \mathrm{d}x x^j f^q(x), \quad f_j^{\mathrm{G}} = \int_{-1}^{1} \mathrm{d}x x^{j-1} f^{\mathrm{G}}(x). \tag{47}$$

The inverse Mellin transform reads

$$f^q(x) = \frac{1}{2\pi i} \int_{c-i\infty}^{c+i\infty} \mathrm{d}j x^{-j-1} f_j^q, \quad f^{\mathrm{G}}(x) = \frac{1}{2\pi i} \int_{c-i\infty}^{c+i\infty} \mathrm{d}j x^{-j} f_j^{\mathrm{G}}, \tag{48}$$

where the integration contour is chosen to lie to the right of all singularities of the PDF moments.

For details refer to [26] and references therein.

5.1 Generalized parton distributions

The goal of this section is to find the conformal moments of GPDs and to calculate the inverse transformation in order to recover GPDs in the x space. We follow the derivation in [27].

The conformal moments of quark and gluons are given by

$$F_n^q\left(\xi, \Delta^2\right) = \int_{-1}^{1} \mathrm{d}x c_n^{3/2}(x,\xi) F^q\left(x, \xi, \Delta^2\right), \tag{49}$$

$$F_n^{\mathrm{G}}\left(\xi, \Delta^2\right) = \int_{-1}^{1} \mathrm{d}x c_{n-1}^{5/2}(x,\xi) F^{\mathrm{G}}\left(x, \xi, \Delta^2\right), \tag{50}$$

where the coefficients c_n^λ contain Gegenbauer polynomials and normalization factors which recover the Mellin moments of PDFs in the forward limit. The coefficients for quarks and gluons are given as

$$c_n^{3/2}(x,\xi) = \xi^n \frac{\Gamma\left(3/2\right)\Gamma(n+1)}{2^n \Gamma\left(n+3/2\right)} C_n^{3/2}\left(\frac{x}{\xi}\right), \tag{51}$$

$$c_{n-1}^{5/2}(x,\xi) = \xi^{n-1} \frac{\Gamma\left(3/2\right)\Gamma(n+1)}{2^n \Gamma\left(n+3/2\right)} \frac{3}{n} C_{n-1}^{5/2}\left(\frac{x}{\xi}\right), \tag{52}$$

which we combine into a single expression

$$c_n^\lambda(x,\xi) = \xi^n \frac{\Gamma(\lambda)\Gamma(n+1)}{2^n \Gamma(n+\lambda)} C_n^\lambda\left(\frac{x}{\xi}\right), \quad \lim_{\xi\to 0} c_n^\lambda(x,\xi) = x^n. \tag{53}$$

To study quarks and gluons simultaneously, we utilize the notation

$$F_n^A\left(\xi, \Delta^2\right) = \int_{-1}^{1} \mathrm{d}x c_n^\lambda(x,\xi) F^A\left(x, \xi, \Delta^2\right), \tag{54}$$

where $A \in \{q, \mathrm{G}\}$ and $\lambda \in \{3/2, 5/2\}$.

In order to reconstruct GPDs from their conformal moments, we use the fact that the Gegenbauer polynomials are orthogonal in the central region $[-\xi, \xi]$ with the weight function $(1-x^2)^{\lambda-1/2}$. We introduce polynomials p_n^λ, which contain the weight and normalization, in order to define the orthogonality relation

$$\int_{-\xi}^{\xi} \mathrm{d}x c_n^\lambda(x,\xi) p_m^\lambda(x,\xi) = (-1)^n \delta_{mn}, \tag{55}$$

where the polynomials explicitly read

$$p_n^\lambda(x,\xi) = \frac{1}{\xi^{n+1}} \frac{2^{n-2\lambda}\Gamma(n+\lambda)}{\Gamma(\lambda)\Gamma(n+1)} \frac{1}{N_k^\lambda} C_n^\lambda\left(-\frac{x}{\xi}\right) \left[1 - \left(\frac{x}{\xi}\right)^2\right]^{\lambda-\frac{1}{2}}. \tag{56}$$

The definition of these polynomials allows us to expand GPDs in terms of Gegenbauer polynomials as

$$F^A\left(x, \xi, \Delta^2\right) = \sum_{n=0}^{\infty} (-1)^n p_n^\lambda(x,\xi) F_n^A\left(\xi, \Delta^2\right). \tag{57}$$

Note that this expansion is defined in the central region only, which means that it diverges for $|\xi| < 1$ when $n \to \infty$ due to the factor ξ^{-n-1}. This means that terms for high n can have a high contribution to the GPD and the series cannot be truncated. The issue is solved by performing a Sommerfeld-Watson transformation, which replaces the infinite sum with a contour integral in the complex plane that includes the positive real axis. We consider the unphysical region $\xi > 1$ and replace the integer indices n with the continuous complex variable j, which yields

$$F^A\left(x,\xi,\Delta^2\right) = \frac{1}{2i}\oint_{(0)}^{(\infty)} \mathrm{d}j \frac{1}{\sin(\pi j)} p_j^\lambda(x,\xi) F_j^A\left(\xi,\Delta^2\right). \tag{58}$$

Using Cauchy's residue theorem and the fact that the function $1/\sin(\pi j)$ has poles at $j \in \mathbb{N}_0$ with residues $(-1)^j/\pi$, we can easily show that (58) coincides with (57) if there are no other singularities inside the contour of the integral. The task now lies in finding the appropriate analytic continuation of the functions p_j^λ and f_j^A in order to obtain the resummation in the unphysical region as well.

The polynomials p_j can be written using the Schläfli integral

$$p_j^\lambda(x,\xi) = (-1)^{\lambda-\frac{1}{2}} \frac{\Gamma(j+\lambda+1)}{\Gamma\left(1/2\right)\Gamma\left(j+\lambda+1/2\right)} \cdot \frac{1}{2\pi i}\oint_{(-1+\epsilon)}^{(1-\epsilon)} \mathrm{d}u \frac{\left(u^2-1\right)^{j+\lambda-\frac{1}{2}}}{(x+u\xi)^{j+1}}, \tag{59}$$

where the integration contour is a unit circle with points ± 1 included. The previous equation can be solved in terms of the hypergeometric function ${}_2F_1$ as

$$p_j^\lambda(x,\xi) = \theta(\xi-|x|)\xi^{-j-1}\mathcal{P}_j^\lambda\left(\frac{x}{\xi}\right) + \theta(x-\xi)\xi^{-j-1}Q_j^\lambda\left(\frac{x}{\xi}\right), \tag{60}$$

where

$$\mathcal{P}_j^\lambda(y) = \frac{2^{j+\lambda-1/2}\Gamma(j+\lambda+1)}{\Gamma\left(1/2\right)\Gamma(j+1)\Gamma\left(\lambda+1/2\right)}(1+y)^{\lambda-1/2}{}_2F_1\left(\begin{array}{cc} -j-\lambda+1/2 & j+\lambda+1/2 \\ \lambda+1/2 & \end{array}\middle|\frac{1+y}{2}\right), \tag{61}$$

$$Q_j^\lambda(y) = -\frac{\sin(\pi j)}{\pi} y^{-j-1}{}_2F_1\left(\begin{array}{cc} (j+1)/2 & (j+2)/2 \\ j+\lambda+1 & \end{array}\middle|\frac{1}{y^2}\right). \tag{62}$$

On the crossover line these polynomials reduce to

$$p_j^\lambda(x,\xi=x) = (-1)^{\lambda+1/2}2^{j+2\lambda-1}x^{-j-1}\frac{\Gamma\left(\lambda-1/2\right)\Gamma(j+\lambda+1)}{\Gamma\left(1/2\right)\Gamma(j+2\lambda)}\frac{\sin\left[\pi\left(j+\lambda-1/2\right)\right]}{\pi}, \tag{63}$$

and for zero skewness to

$$p_j^\lambda(x,\xi=0) = (-1)^{\lambda+1/2}x^{-j-1}\frac{\sin\left[\pi\left(j+\lambda-1/2\right)\right]}{\pi}. \tag{64}$$

Up to a few prefactors, this is the integral kernel for the inverse Mellin moments, which should be the case because in the forward limit we need to recover PDFs.

The general Mellin-Barnes representation of GPDs is given as

$$F^q\left(x,\xi,\Delta^2\right) = \frac{1}{2\pi i}\int_{c-i\infty}^{c+i\infty} \mathrm{d}j \frac{p_j^{3/2}(x,\xi)}{\sin(\pi j)} F_j^q\left(\xi,\Delta^2\right), \tag{65}$$

$$F^{\mathrm{G}}\left(x,\xi,\Delta^2\right) = \frac{1}{2\pi i}\int_{c-i\infty}^{c+i\infty} \mathrm{d}j \frac{p_{j-1}^{5/2}(x,\xi)}{\sin(\pi j)} F_j^{\mathrm{G}}\left(\xi,\Delta^2\right), \tag{66}$$

where the polynomials are given in (60).

We have managed to reconstruct the GPDs in the x-space from conformal moments using analytic continuation. The study of GPDs in the conformal space can be useful because the evolution is simpler, it is multiplicative as opposed to it being a convolution, which is numerically easier to treat.

6 Mellin-Barnes representation of scattering amplitudes

In this section we study the scattering amplitudes of DVCS and DVMP, which contain convolutions of GPDs with the corresponding hard scattering part of the amplitude. The Mellin-Barnes representation of GPDs can be used to directly calculate CFFs and TFFs without having to first obtain GPDs in the x-space. As a primer, we observe structure functions which are also written as convolutions of PDFs and the hard scattering part of the amplitude in the forward limit.

6.1 Compton form factors

Compton form factors appear in the DVCS amplitude and due to the factorization theorem, can be written as a convolution of the hard and soft scattering parts. The soft parts are GPDs, and in this chapter we use their Mellin-Barnes representation in order to expand the CFFs in conformal partial waves. The uniqueness of the analytic continuation $n \to j$ is guaranteed by Carlson's theorem [28].

We start with the quark CFFs at LO

$$\mathcal{F}^q\left(\xi,\Delta^2,Q^2\right)=\int_{-1}^{1}\mathrm{d}x\left[\frac{1}{\xi-x-i\epsilon}\mp\frac{1}{\xi+x-i\epsilon}\right]F^q\left(x,\xi,\Delta^2,Q^2\right), \tag{67}$$

where the minus sign corresponds to the vector CFFs, and the plus sign corresponds to axial-vector CFFs. Writing the GPDs in terms of quark and antiquark distributions and using the Mellin-Barnes representation, we can integrate out the x dependence and write [27]

$$\mathcal{F}^q\left(\xi,\Delta^2,Q^2\right)=\frac{1}{2i}\int_{c-i\infty}^{c+i\infty}\mathrm{d}j\xi^{-j-1}\frac{2^{j+1}\Gamma\left(j+5/2\right)}{\Gamma\left(3/2\right)\Gamma(j+3)}\left[i\pm\left\{\begin{array}{c}\tan\\ \cot\end{array}\right\}\left(\frac{\pi j}{2}\right)\right]F_j^q\left(\xi,\Delta^2,Q^2\right). \tag{68}$$

This can easily be expanded to include higher orders in perturbation theory, so we can write

$$\mathcal{F}^q\left(\xi,\Delta^2,Q^2\right)=\frac{1}{2i}\int_{c-i\infty}^{c+i\infty}\mathrm{d}j\xi^{-j-1}\frac{2^{j+1}\Gamma\left(j+5/2\right)}{\Gamma\left(3/2\right)\Gamma(j+3)}\left[i\pm\left\{\begin{array}{c}\tan\\ \cot\end{array}\right\}\left(\frac{\pi j}{2}\right)\right]{}^qc_j^{\mathrm{I}}F_j^q\left(\xi,\Delta^2,Q^2\right). \tag{69}$$

We adopt the convention for expansion of the hard-scattering coefficients in terms of the strong coupling constant

$${}^qc_j^{\mathrm{I}}\left(\alpha_{\mathrm{s}}\left(\mu_{\mathrm{R}}\right),\frac{Q^2}{\mu_{\mathrm{F}}^2}\right)={}^qc_j^{\mathrm{I}(0)}+\frac{\alpha_{\mathrm{s}}^2\left(\mu_{\mathrm{R}}\right)}{2\pi}{}^qc_j^{\mathrm{I}(1)}\left(\alpha_{\mathrm{s}}\left(\mu_{\mathrm{R}}\right),\frac{Q^2}{\mu_{\mathrm{F}}^2}\right)+\mathcal{O}\left(\alpha_{\mathrm{s}}^4\right). \tag{70}$$

6.2 Transition form factors

We now apply the same procedure for the Mellin-Barnes representation of transition form factors, which appear in the cross section of DVMP. Here we have an additional complication because of the presence of distribution amplitudes. We have shown the expansion of DAs and GPDs in terms of conformal moments, so we write the TFFs as an infinite sum over the conformal moments

$$\mathcal{F}^{q(\pm)}\left(\xi,\Delta^2,Q^2\right)=\frac{fC_{\mathrm{F}}}{QN_{\mathrm{c}}}\sum_{n,k=0}^{\infty}\xi^{-n-1}\varphi_k\left(\mu_\varphi^2\right){}^qT_{nk}^{\mathrm{I}}\left(\frac{Q^2}{\mu_{\mathrm{F}}^2},\frac{Q^2}{\mu_\varphi^2},\frac{Q^2}{\mu_{\mathrm{R}}^2}\right)F_n^{q(\pm)}\left(\xi,\Delta^2,\mu_{\mathrm{F}}^2\right), \tag{71}$$

$$\mathcal{F}^{\mathrm{G}}\left(\xi,\Delta^2,Q^2\right)=\frac{f}{QN_{\mathrm{c}}}\sum_{n,k=0}^{\infty}\xi^{-n-1}\varphi_k\left(\mu_\varphi^2\right){}^{\mathrm{G}}T_{nk}^{\mathrm{I}}\left(\frac{Q^2}{\mu_{\mathrm{F}}^2},\frac{Q^2}{\mu_\varphi^2},\frac{Q^2}{\mu_{\mathrm{R}}^2}\right)F_n^{\mathrm{G}}\left(\xi,\Delta^2,\mu_{\mathrm{F}}^2\right). \tag{72}$$

Note that we now have a dependence on the factorization scale of the DA, so we denote the factorization scales for GPDs (μ_{F}) and DAs (μ_ϕ) differently.

In the case of TFFs, as opposed to CFFs, we have an addition of DAs and their evolution. By expanding the DA in terms of conformal moments, often only a finite number of effective conformal moments is taken into consideration, so at LO in evolution we have a finite sum. At NLO, there is a mixing between DA moments, which introduces another infinite sum. Since higher conformal moments are suppressed, this sum is in practice truncated. In practice one often takes the inital scales of GPDs and DAs to be the same, i.e. $\mu_0=\mu_0'$.

The TFFs can be written as

$$\mathcal{F}^A\left(\xi,\Delta^2,Q^2\right)=\frac{fC_{\mathrm{F}}}{QN_{\mathrm{c}}}\frac{1}{2i}\int_c\mathrm{d}j\xi^{-j-1}\left[i\pm\left\{\begin{array}{c}\tan\\ \cot\end{array}\right\}\left(\frac{\pi j}{2}\right)\right]\varphi_k\left(\mu_0^2\right)\underset{\text{even}}{\overset{k}{\oplus}}\overline{T}_{jk}^{\mathrm{I}}\left(Q^2,\mu_0^2\right)F_j^A\left(\xi,\Delta^2,\mu_0^2\right), \tag{73}$$

where $\overset{k}{\oplus}$ denotes the summation over the index k, and the factor coming from the color structure is

$$C_F=\frac{N_{\mathrm{c}}^2-1}{2N_{\mathrm{c}}}. \tag{74}$$

It is worth noting that the expressions for CFFs and TFFs derived in this chapter incorporate the dispersion relation (41) without the subtraction constant.

7 Modeling GPDs

In this chapter we will present our approach to modeling GPDs in the conformal space, which will be utilized in simultaneous global fits to DIS, DVCS and DVMP at low x. Much of our assumptions will rely on conclusions drawn from Regge theory and studies performed on PDFs.

We have seen that GPDs depend on three variables, which we choose to be x, ξ and t. When we expand the x-space GPDs in the conformal space, the GPD conformal moments depend on ξ and t. We adopt the approach where the skewness dependence is expanded via t-channel SO(3) partial waves, meaning that our GPDs have a double partial wave (PW) expansion. Formally we have

$$F_j^a(\xi,t) = \sum_{\substack{J=J_{\min}\\ \text{even}}}^{j+1} F_{j,J}^a(t)\xi^{j+1-J}\hat{d}^J_{\alpha,\beta}(\xi), \quad J = j+1, j-1, j-3, \ldots, \quad a \in \{q, \mathrm{G}\}, \tag{75}$$

where J is the angular momentum in the t-channel, and $\hat{d}^J_{\alpha,\beta}(\xi)$ are the crossed version of Wigner's reduced rotation matrices. The reason we call this a t-channel expansion is that it comes about naturally in the process which is the crossed process of DVCS. If we write DVCS symbolically as a virtual photon scattering off a hadron in the s-channel

$$\gamma^*(q) + h(p) \to \gamma\left(q'\right) + h\left(p'\right), \tag{76}$$

its t-channel counterpart is the process

$$\gamma^*(q) + \gamma\left(-q'\right) \to h\left(p'\right) + \bar{h}(-p). \tag{77}$$

Here the scattering amplitude is given by meson GPDs, which can be expanded into irreducible SO(3) representations labeled by the orbital angular momentum quantum number. By crossing this expansion back onto DVCS, we need to introduce the substitution

$$\cos\theta_t \to -\frac{1}{\xi} + \mathcal{O}\left(1/Q^2\right), \tag{78}$$

where θ_t is the t-channel center-of-mass scattering angle. We can therefore describe a process in the $s-$channel by an exchange in the t-channel.

The partial wave amplitude $F_{j,j+1}$ is the Mellin moment of the zero-skewness GPD, and the subleading amplitudes, with J smaller than $j+1$, are suppressed by the factor ξ^{j+1-J}. By considering helicities and spins of the involved particles, one can conclude that two Wigner matrices contribute to the expansion (75), $\hat{d}^J_{0,0}$ and $\hat{d}^J_{0,1}$, which are given in terms of the Gegenbauer polynomials with indices 1/2 and 3/2, respectively. Equivalently, they can also be expressed in terms of the hypergeometric function ${}_2F_1$

$$\hat{d}^J_{0,0}(\xi) = \frac{\Gamma\left(1/2\right)\Gamma(J+1)}{2^J\Gamma\left(J+1/2\right)}\xi^J C_J^{1/2}\left(\frac{1}{\xi}\right) = \frac{\Gamma\left(1/2\right)\Gamma(J+1)}{2^J\Gamma\left(J+1/2\right)}\xi^J {}_2F_1\left(\begin{array}{cc} -J & J+1 \\ & 1 \end{array}\middle|\frac{\xi-1}{2\xi}\right), \tag{79}$$

$$\hat{d}^J_{0,1}(\xi) = \frac{\Gamma\left(1/2\right)\Gamma(J)}{2^J\Gamma\left(J+1/2\right)}\xi^{J-1} C_{J-1}^{3/2}\left(\frac{1}{\xi}\right) = \frac{\Gamma\left(3/2\right)\Gamma(J+1)}{2^J\Gamma\left(J+1/2\right)}\xi^{J-1} {}_2F_1\left(\begin{array}{cc} -J+1 & J+2 \\ & 2 \end{array}\middle|\frac{\xi-1}{2\xi}\right). \tag{80}$$

We can find a basis where the amplitudes do not mix, which are linear combinations of GPDs H_j and E_j. The t-channel helicity conserving, or "electric" combination [29]

$$H_j^a + \frac{t}{4M^2}E_j^a, \quad a \in \{q, \mathrm{G}\} \tag{81}$$

is given in terms of $\hat{d}^J_{0,0}$, and the t-channel helicity flip, or "magnetic" combination

$$H_j^a + E_j^a, \quad a \in \{q, \mathrm{G}\} \tag{82}$$

is given in terms of $\hat{d}^J_{0,1}$.

For more details see [30, 31] and references therein. It was shown in [30] that for the kinematics we are interested in, roughly $\xi \leq 0.3$, which corresponds to $x \leq 0.46$, we can approximate the coefficients in the expansion (75) as

$$\hat{d}^J_{\alpha,\beta}(\xi) \approx 1. \tag{83}$$

In the forward limit $\xi = 0$, the leading amplitude in the PW expansion should reduce to the Mellin moment of the corresponding PDF

$$F^a_{j,j+1}(0) = f_j^a = \int_0^1 \mathrm{d}x x^j f^a(x). \tag{84}$$

This prompts us to use the known PDF ansatz to model the leading amplitude in the PW expansion. But in this approach we do not use state-of-the-art results for PDFs obtained from experiment, since current methods for modeling PDFs are more sophisticated than our approach and could lead to inconsistencies. Instead, we use a well-known ansatz for PDFs

$$f^a(x) = \frac{N_a}{B\left(2-\alpha_0^a, \beta^a+1\right)} x^{-\alpha_0^a}(1-x)^{\beta^a}, \tag{85}$$

which in the conformal space corresponds to

$$f_j^a = N_a \frac{B\left(1-\alpha_0^a+j, \beta^a+1\right)}{B\left(2-\alpha_0^a, \beta^a+1\right)}. \tag{86}$$

The $1-x$ part of the PDF describes its high x behavior, which we cannot access in our analysis. We therefore rely on counting rules to fix $\beta^{\text{sea}} = 8$ and $\beta^{\text{G}} = 6$. In (85) and (86) the normalization is chosen so that N_a corresponds to the average longitudinal momentum fraction of parton a. All of these factors need to sum up to 1, i.e.

$$N_{\text{sea}} + N_{\text{val}} + N_{\text{G}} = 1. \tag{87}$$

In order to introduce the t dependence, which factorizes from the x dependence at low x [32], we take note from Regge phenomenology to complete the Regge trajectory

$$\alpha_0^a \to \alpha^a(t) = \alpha_0^a + \alpha'^a t. \tag{88}$$

We use this trajectory to decorate the forward GPDs with a factor

$$\frac{1}{1-\dfrac{t}{(m_j^a)^2}}, \quad (m_j^a)^2 = \frac{1+j-\alpha_0^a}{\alpha'^a}. \tag{89}$$

Regge theory tells us that at high energies the scattering amplitude behaves as $\Gamma(-\alpha(t))s^{\alpha(t)}$, where $\alpha(t)$ is a trajectory in the complex j space which contains all particles in the t-channel exchange, and for each of these particles $\alpha(t) = j+1$, where j is a non-negative integer. The exchange of these particles induces poles in the amplitude and these poles are here modeled as a monopole factor (89). We then add a residual t-dependence in the form of a dipole impact factor

$$\beta(t) = \left(1-\frac{t}{m_a^2}\right)^{-2}, \tag{90}$$

where we ignore all j dependence of the mass parameter m_a^2 since this dependence cannot be discerned at low x.

The final GPD form is therefore

$$F_{j,j+1}^a(t) \equiv f_j^a(t) = f_j^a \frac{1+j-\alpha_0^a}{1+j-\alpha_0^a-\alpha'^a t}\left(1-\frac{t}{m_a^2}\right)^{-2}, \tag{91}$$

with f_j^a given in (86). Another possibility for the residual t-dependence is an exponential function

$$\beta(t) = e^{Bt}, \tag{92}$$

but it is unlikely that such a t-dependence would come about naturally from a field theoretical standpoint. However, for low values of x both of the residual functions similarly reproduce data.

Using previous analyses, it was shown that the data we will be working with does not distinguish between the t dependencies of the different partial waves, and that the description works sufficiently well by truncating (75) after the second subleading PW [33]. Our full model is therefore

$$F_j^a(\xi,t) = \left(1+s_2^a\xi^2+s_4^a\xi^4\right) f_j^a(t), \tag{93}$$

where the parameters s_2 and s_4 are determined in fits. In the Mellin-Barnes representation we can shift the terms in the subleading partial waves by $j \to j-2$ and $j \to j-4$ so that we can write the CFFs/TFFs as

$$\boldsymbol{\mathcal{F}} = \frac{1}{2i}\int_{c-i\infty}^{c+i\infty} \mathrm{d}j \xi^{-j-1}\left[i+\tan\left(\frac{\pi j}{2}\right)\right]\left[\overline{\boldsymbol{T}}_j^{\text{I}} + \boldsymbol{s_2}\overline{\boldsymbol{T}}_{j+2}^{\text{I}} + \boldsymbol{s_4}\overline{\boldsymbol{T}}_{j+4}^{\text{I}}\right]\boldsymbol{F}_j. \tag{94}$$

In the former expression the subtraction constant is set to zero, since for such a small range of kinematic variable values we cannot extract its form.

In order to control the convergence of the integrand and simplify numerical integration, the integration contour can be deformed by introducing

$$j = c + ye^{i\phi}, \tag{95}$$

where y is now the integration variable. We do this in order to dampen the integrand for large values of y due to the factor $x^{-y\exp(i\phi)}$, which can be accomplished by choosing $\phi > \pi/2$. The original contour is recovered for $\phi = \pi/2$. The deformed contour is represented in figure 8 below.

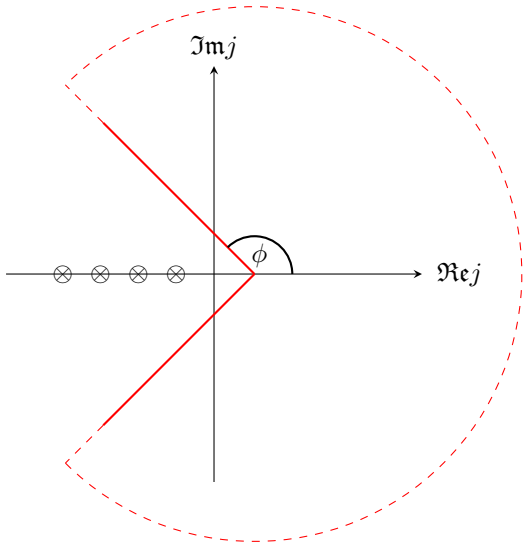

Figure 8: Deformed integral contour of the Mellin-Barnes integral.

The choice of ϕ and c should not change the final result, but care must be taken to avoid any poles coming from GPD moments or the evolution operator, which are depicted in Figure 8 with $\otimes$ symbols.

Finally, the Schwarz reflection principle can be used to integrate only over one of the legs in the deformed contour

$$\begin{aligned}\mathcal{F}^A\left(\xi,\Delta^2,\mathcal{Q}^2\right) =& \mathfrak{Im} e^{i\phi}\int_0^\infty \mathrm{d}y \xi^{-j-1}\tan\left(\frac{\pi j}{2}\right)\boldsymbol{C}_j\left(Q^2/\mu^2,\alpha_s(\mu)\right)\boldsymbol{F}_j^A\left(\xi,\Delta^2,\mu^2\right)\\ &+ i\mathfrak{Im} e^{i\phi}\int_0^\infty \mathrm{d}y \xi^{-j-1}\boldsymbol{C}_j\left(Q^2/\mu^2,\alpha_s(\mu)\right)\boldsymbol{F}_j^A\left(\xi,\Delta^2,\mu^2\right)\Big|_{j=c+ye^{i\phi}}.\end{aligned} \tag{96}$$

This model was used to simultaneously fit DIS, DVCS and DVMP HERA data, which is low-x and high Q^2 data consisting of unpolarized cross section without the lepton part, and the structure function F_2 in case of DIS. Results are published in [34].

All of this theory is implemented in a software called Gepard, which is available to download as a Python package, and the tutorial is available at: https://gepard.phy.hr/index.html.

7.1 Hybrid models

Since JLab data is not measured at low x and high Q^2 like HERA data, we cannot make the same approximations as in the previous chapter. Specifically, in this study we cannot ignore the valence quark sector, nor the presence of CFFs other than $\mathcal{H}$. The model presented in this section was detailed in [33, 35, 36], and is denoted as `KM` in most instances.

Given that our computer codes do not have the valence sector implemented in the conformal space, the model is a hybrid one. The valence sector is modeled in the x-space on the crossover line $x = \eta$

$$H_q^{\mathrm{val}}(x,x,t) = \frac{n_q r_q}{1+x}\left(\frac{2x}{1+x}\right)^{-\alpha_v(t)}\left(\frac{1-x}{1+x}\right)^{b_q}\frac{1}{1-\frac{1-x}{1+x}\frac{t}{M_q^2}}, \quad q = u,d. \tag{97}$$

This model is based on the same arguments made for the conformal moments of GPDs. Now the Regge trajectory is not a parameter, but is given by the Reggeon exchange

$$\alpha_v(t) = 0.43 + 0.85 t/\mathrm{GeV}^2. \tag{98}$$

The parameter n_q is the normalization known from PDF studies, and r^q parametrizes the skewness ratio

$$r^a\left(Q^2\right) = \frac{H^a\left(x,\xi=x,t=0,Q^2\right)}{H^a\left(x,\xi=0,t=0,Q^2\right)}. \tag{99}$$

We argued the use of conformal moments in our description of GPDs due to easier implementation of evolution. Given the difficulties, we do not implement QCD evolution in the valence sector, and we also remain at the LO level, where the imaginary part of the valence CFF $\mathcal{H}$ is given simply as

$$\mathfrak{Im}\mathcal{H}^{\text{val}}(\xi,t) = \pi \sum_{q=u,d} Q_q^2 \left[H_q^{\text{val}}(\xi,\xi,t) - H_q^{\text{val}}(-\xi,\xi,t)\right]. \tag{100}$$

For the analysis of proton data, a simple model was used $F_u^{\text{val}} = 2F_d^{\text{val}}$.

This model also includes dispersion relations, where we cannot ignore the subtraction constant. We model it separately as

$$\Delta_{\mathcal{F}}(t) = \frac{C}{\left(1 - \frac{t}{M_C^2}\right)^2}, \tag{101}$$

also ignoring its dependence on Q^2. The implementation of dispersion relations allows us to model only the imaginary parts of CFFs and one subtraction constant, since $\Delta_{\mathcal{H}} = -\Delta_{\mathcal{E}}$ and $\Delta_{\widetilde{\mathcal{H}}} = \Delta_{\widetilde{\mathcal{E}}} = 0$. In principle, this reduces the number of functions to model from 8 to 5, and the subtraction constant depends only on one kinematic variable. The free parameters of this sector are therefore r_q, b_q, M_q, C and M_C.

The sea quark and gluon GPDs are modeled in the conformal space as explained before, also at LO to match the valence sector, with the QCD evolution implemented.

By observing Table 2, we can see that the influence of CFFs $\mathcal{E}$ and $\widetilde{\mathcal{E}}$ is kinematically suppressed in most proton DVCS observables, therefore in our models we set $\mathfrak{Im}\mathcal{E}$ and $\mathfrak{Im}\widetilde{\mathcal{E}}$ to zero. This is not to say that these CFF components are small, but rather that they are not accessible from the data we are observing. The real component of the CFF $\mathcal{E}$ is given by the subtraction constant $-\Delta_{\mathcal{H}}$, but the CFF $\widetilde{\mathcal{E}}$ has an additional contribution from the pion pole, which yields a real contribution. This phenomenon occurs due to an exchange of a virtual pion inside the nucleon, which decays into the $q\overline{q}$ pair probed by the photon in the ERBL region. For small $|t|$, the pion is only weakly off-shell, and for $t = m_\pi^2$ we have an exchange of an on-shell particle, which results in a pole contribution because the pion propagator diverges. The pion pole contribution is equal to [37]

$$\mathfrak{Re}\widetilde{\mathcal{E}} = \frac{1}{\xi}\frac{2g_A M^2 r_\pi}{m_\pi^2 - t}\frac{1}{\left(1 - \frac{t}{M_\pi^2}\right)^2}. \tag{102}$$

Here $g_A \approx 1.26$ is the axial charge of the nucleon, M is the nucleon mass, m_π is the mass of the pion expressed in GeV, and M_π is a free parameter. In the case of the neutron, this contribution has an opposite sign. This model therefore parametrizes 3 CFF components and one subtraction constant.

References

[1] Marija Čuić. *Imaging of the three-dimensional quark-gluon structure of the proton via analysis of deeply virtual electron scattering*. PhD thesis, Zagreb U., Phys. Dept., 2024.

[2] A.V. Belitsky, D. Müller, and A. Kirchner. Theory of deeply virtual compton scattering on the nucleon. *Nuclear Physics B*, 629(1):323–392, 2002.

[3] John C. Collins and Andreas Freund. Proof of factorization for deeply virtual compton scattering in qcd. *Phys. Rev. D*, 59:074009, Feb 1999.

[4] Brandon Kriesten, Simonetta Liuti, Liliet Calero-Diaz, Dustin Keller, Andrew Meyer, Gary R. Goldstein, and J. Osvaldo Gonzalez-Hernandez. Extraction of Generalized Parton Distribution Observables from Deeply Virtual Electron Proton Scattering Experiments. *Phys. Rev. D*, 101(5):054021, 2020.

[5] John C. Collins, Leonid Frankfurt, and Mark Strikman. Factorization for hard exclusive electroproduction of mesons in qcd. *Phys. Rev. D*, 56:2982–3006, Sep 1997.

[6] Leonid Frankfurt, Werner Koepf, and Mark Strikman. Hard diffractive electroproduction of vector mesons in qcd. *Phys. Rev. D*, 54:3194–3215, Sep 1996.

[7] Leonid Frankfurt, Werner Koepf, and Mark Strikman. Diffractive heavy quarkonium photoproduction and electroproduction in qcd. *Phys. Rev. D*, 57:512–526, Jan 1998.

[8] L. L. Frankfurt, P. V. Pobylitsa, M. V. Polyakov, and M. Strikman. Hard exclusive pseudoscalar meson electroproduction and spin structure of the nucleon. *Phys. Rev. D*, 60:014010, Jun 1999.

[9] L. L. Frankfurt, M. V. Polyakov, M. Strikman, and M. Vanderhaeghen. Hard exclusive electroproduction of decuplet baryons in the large N_c limit. *Phys. Rev. Lett.*, 84:2589–2592, Mar 2000.

[10] L. Mankiewicz, G. Piller, and A. Radyushkin. Hard exclusive electroproduction of pions. *Eur. Phys. J. C*, 10:307–312, 1999.

[11] L. Mankiewicz, G. Piller, and T. Weigl. Hard exclusive meson production and nonforward parton distributions. *Eur. Phys. J. C*, 5:119–128, 1998.

[12] L. Mankiewicz, G. Piller, and T. Weigl. Hard leptoproduction of charged vector mesons. *Phys. Rev. D*, 59:017501, Dec 1998.

[13] A.V. Radyushkin. Asymmetric gluon distributions and hard diffractive electroproduction. *Physics Letters B*, 385(1):333–342, 1996.

[14] A.V. Belitsky and D. Müller. Hard exclusive meson production at next-to-leading order. *Physics Letters B*, 513(3):349–360, 2001.

[15] M. Diehl and W. Kugler. Next-to-leading order corrections in exclusive meson production. *Eur. Phys. J. C*, 52:933–966, 2007.

[16] D. Yu. Ivanov, L. Szymanowski, and G. Krasnikov. Vector meson electroproduction at next-to-leading order. *JETP Lett.*, 80:226–230, 2004. [Erratum: JETP Lett. 101, 844 (2015)].

[17] D. Müller, T. Lautenschlager, K. Passek-Kumerički, and A. Schäfer. Towards a fitting procedure to deeply virtual meson production – the next-to-leading order case. *Nuclear Physics B*, 884:438–546, 2014.

[18] G. Duplančić, D. Müller, and K. Passek-Kumerički. Next-to-leading order corrections to deeply virtual production of pseudoscalar mesons. *Physics Letters B*, 771:603–610, 2017.

[19] Edgar R. Berger, M. Diehl, and B. Pire. Time - like Compton scattering: Exclusive photoproduction of lepton pairs. *Eur. Phys. J. C*, 23:675–689, 2002.

[20] M. Guidal and M. Vanderhaeghen. Double deeply virtual compton scattering off the nucleon. *Phys. Rev. Lett.*, 90:012001, Jan 2003.

[21] A. V. Belitsky and D. Müller. Exclusive electroproduction of lepton pairs as a probe of nucleon structure. *Phys. Rev. Lett.*, 90:022001, Jan 2003.

[22] B. Pire, L. Szymanowski, and J. Wagner. Next-to-leading order corrections to timelike, spacelike, and double deeply virtual compton scattering. *Phys. Rev. D*, 83:034009, Feb 2011.

[23] I. V. Anikin and O. V. Teryaev. Dispersion relations and subtractions in hard exclusive processes. *Phys. Rev. D*, 76:056007, Sep 2007.

[24] M. Diehl and D. Yu. Ivanov. Dispersion representations for hard exclusive processes: beyond the Born approximation. *Eur. Phys. J. C*, 52:919–932, 2007.

[25] Peter Kroll, Herve Moutarde, and Franck Sabatie. From hard exclusive meson electroproduction to deeply virtual Compton scattering. *Eur. Phys. J. C*, 73(1):2278, 2013.

[26] Tobias Lautenschlager. *Towards a global estimate for generalized parton distributions*. Phd thesis, University of Regensburg, August 2015.

[27] D. Müller and A. Schäfer. Complex conformal spin partial wave expansion of generalized parton distributions and distribution amplitudes. *Nuclear Physics B*, 739(1):1–59, 2006.

[28] Fritz Carlson. *Sur une classe de séries de Taylor*. Phd thesis, Uppsala University, 1914.

[29] M. Diehl. Generalized parton distributions. *Physics Reports*, 388(2):41–277, 2003.

[30] K. Kumerički, D. Müller, and K. Passek-Kumerički. Towards a fitting procedure for deeply virtual compton scattering at next-to-leading order and beyond. *Nuclear Physics B*, 794(1):244–323, 2008.

[31] Dieter Müller, Maxim V. Polyakov, and Kirill M. Semenov-Tian-Shansky. Dual parametrization of generalized parton distributions in two equivalent representations. *JHEP*, 03:052, 2015.

[32] D.S. Hwang and D. Müller. Implication of the overlap representation for modelling generalized parton distributions. *Physics Letters B*, 660(4):350–359, 2008.

[33] Krešimir Kumerički and Dieter Müller. Deeply virtual compton scattering at small xb and the access to the gpd h. *Nuclear Physics B*, 841(1):1–58, 2010.

[34] Marija Čuić, Goran Duplančić, Krešimir Kumerički, and Kornelija Passek-K. NLO corrections to the deeply virtual meson production revisited: impact on the extraction of generalized parton distributions. *JHEP*, 12:192, 2023.

[35] Krešimir Kumerički, Dieter Müller, and Morgan Murray. HERMES impact for the access of Compton form factors. *Phys. Part. Nucl.*, 45(4):723–755, 2014.

[36] Krešimir Kumerički and Dieter Müller. Description and interpretation of dvcs measurements*. *EPJ Web of Conferences*, 112:01012, 2016.

[37] M. Penttinen, M. V. Polyakov, and K. Goeke. Helicity skewed quark distributions of the nucleon and chiral symmetry. *Phys. Rev. D*, 62:014024, Jun 2000.